

# Polymer Chemistry

Accepted Manuscript



This is an *Accepted Manuscript*, which has been through the Royal Society of Chemistry peer review process and has been accepted for publication.

*Accepted Manuscripts* are published online shortly after acceptance, before technical editing, formatting and proof reading. Using this free service, authors can make their results available to the community, in citable form, before we publish the edited article. We will replace this *Accepted Manuscript* with the edited and formatted *Advance Article* as soon as it is available.

You can find more information about *Accepted Manuscripts* in the [Information for Authors](#).

Please note that technical editing may introduce minor changes to the text and/or graphics, which may alter content. The journal's standard [Terms & Conditions](#) and the [Ethical guidelines](#) still apply. In no event shall the Royal Society of Chemistry be held responsible for any errors or omissions in this *Accepted Manuscript* or any consequences arising from the use of any information it contains.

## ARTICLE

# Surface engineered nanogels assembly with integrated blood compatibility, cell proliferation and antibacterial property: towards multifunctional biomedical membrane

Cite this: DOI: 10.1039/x0xx00000x

Received 00th January 2014,  
Accepted 00th January 2014

DOI: 10.1039/x0xx00000x

[www.rsc.org/](http://www.rsc.org/)

Yi Xia,<sup>a,1</sup> Chong Cheng,<sup>a,b,1,\*</sup> Rui Wang,<sup>a</sup> Hui Qin,<sup>a</sup> Yi Zhang,<sup>a</sup> Lang Ma,<sup>a</sup> Hong Tan,<sup>a</sup> Zhongwei Gu,<sup>c</sup> and Changsheng Zhao<sup>a,c,\*</sup>

In this study, novel 3D multifunctional nanolayers are fabricated on biomedical membrane surfaces via layer-by-layer (LBL) self-assembly of nanogels and heparin-like polymers. To integrate long-term antibacterial activity, Ag nanoparticle embedded nanogels were firstly prepared. Then, the Ag-nanogels were assembled onto membrane surfaces by electrostatic interaction. To obtain heparin-mimicking surface, the as-prepared nanogel coated membranes were further assembled with heparin-like polymers by two different processes. The results indicated that the obtained nanogel and heparin-mimicking polymer assembled membranes exhibited 3D surface morphologies. Systematical blood compatibility and antithrombotic evaluation revealed that the functionalized membranes showed increased hydrophilicity, decreased protein adsorption, prolonged clotting times, and greatly suppressed platelet adhesion compared to pristine membrane. The cell observations demonstrated that the pristine, nanogel assembled, and heparin-mimicking membranes showed different performances in endothelial cell proliferation and adhesion morphology. The results of antibacterial study indicated that the functionalized membranes exhibited significant inhibition capability for *Escherichia coli* and *Staphylococcus aureus*. In general, the surface co-assembly of nanogels and heparin-mimicking polymers conferred the functionalized membranes with integrated blood compatibility, cell proliferation and antibacterial properties for multi-applications, which may forward the fabrication of biomedical devices by surface assembly of functional nanogels.

## 1. Introduction

Over the last thirty years, the significance of artificial membranes has been recognized for various biomedical applications, and plenty of commercialized membranes have been used in market varied from disposable filtration membrane to clinical hemodialysis membrane, cardio pulmonary by pass device and other medical equipment.<sup>1, 2</sup> However, during the recent years, several fatal problems for artificial membrane have been revealed: (1) blood components activation and thrombus generation,<sup>3</sup> (2) materials induced cell toxicity, teratogenicity and carcinogenicity,<sup>4, 5</sup> (3) biomaterials induced bacterial infection (it is difficult to be eradicated due to the formation of bacterial biofilm on the membrane surface),<sup>6</sup> (4) long-term inflammation and immunologic rejection of implant materials and the resulted tissue calcification.<sup>7</sup> Most of these problems were resulted from the unfavourable membrane interfaces and/or unreasonable surface design. Therefore, the design of advanced biomedical membranes and their practical utilization are highly depended on the appropriate physical and chemical interface design to approach favourable biological

responses or biocompatibility.<sup>8-11</sup> The ultimate goal for the surface modification of biomedical membranes is to confer them with desired properties, such as the anti-thrombogenic ability, cell compatibility, and long-term antibacterial ability, and thus make the obtained artificial devices suitable for contacting with blood, live tissues and organs both in short-term and long-term applications.<sup>11-13</sup>

Specific functional biointerface design is one of the most important processes to gain insights into the interactions or biological responses between synthetic membranes and living systems. A lot of researches have been carried out to prepare functional membranes with different chemical compositions and physical morphologies along different dimensions.<sup>14-16</sup> These studies have indicated a lot of exciting results and broadened the usages of the membranes or films by integrating new components or functions.<sup>17-19</sup> Particularly, the design of integrated biocompatibility and biofunctionality has attached great attentions for implanted and blood contacted membranes, and various methods have been developed, such as physical blending,<sup>20</sup> surface plasma treatment,<sup>21-23</sup> surface grafting,<sup>24-26</sup> and surface layer-by-layer (LBL) assembly and coating,<sup>27, 28</sup>

etc.. Among the methods, blending of functional polymers or nano/micro-materials has usually been recognized as a convenient method to improve the surface property between membrane and blood (or tissues);<sup>29, 30</sup> whereas, the blending method usually changes the mechanical property of the bulk matrix. Meanwhile, the surface plasma treatment and grafting usually need complex physical or chemical treatment to obtain active functional groups or nano/micro-patterns, and might be not suitable for large-scale surface functionalization of the artificial membranes. Surface LBL assembly and coating are regarded as the most promising strategies to enable blood and tissue contacting materials with specific bioactivity and favourable biocompatibility efficiently, and are harmless to the mechanical property.<sup>31, 32</sup>

Various surface assembly and coating methods have been developed based on multi-covalent and/or noncovalent interactions; meanwhile, various functional building blocks and materials, such as polyelectrolytes,<sup>33, 34</sup> nanoparticles,<sup>35</sup> nanotubes,<sup>36</sup> and nano/microgels,<sup>32, 37-42</sup> have been intensively studied and taken for the surface construction of thin film layers on membrane surfaces, and the modified biomedical membranes show versatile biological functionalities and activities. It has been verified that most of the assembly, such as polyelectrolyte assembly, usually obtains 2D dense surface layer, which may limit the surface density of functional groups and insufficient bioactivity of the modified membranes, and the surface dense layer may lack of ability to mimic the biological functions of living systems.<sup>33</sup> Recent investigations indicate that the surface 3D porous layers assembled by nanomaterials may overcome this inherent drawback by conferring the biointerface with high density of functional and bioactive groups/molecules. Among the numerous nanomaterials, nanogels are promising candidates for designing advanced membranes with integrated 3D morphology and multifunctionality since they are suitable for cargo loading or attachment of various bioactive chemical groups along with well biocompatibility,<sup>42</sup> which have been widely used in drug-delivery systems, regenerative medicine, and bioimaging.<sup>43</sup> Most recently, Xia et al. applied thermoresponsive poly(N-isopropylacrylamide-co-styrene) microgel films for cell growth and detachment via temperature stimuli.<sup>32</sup> Meanwhile, Bajpai and Raju indicated that polymeric hydrogels could provide sustained functional molecule release and fine surface cover for antibacterial reagents,<sup>44, 45</sup> such as Ag nanoparticles (Ag NPs, the direct exposure of Ag NPs presents certain biotoxicity to cells and organs),<sup>46</sup> which have become ideal candidate for the design of advanced antibacterial membranes. With these advantages, Ag NPs embedded nanogels can be taken for the construction of biocompatible membranes with integrated antibacterial property. However, for developing the integrated multiple biofunctionality, the simple assembly of these nanogels is insufficient in some aspects, such as the anti-thrombogenic ability and promotion of cell proliferation. Thus, the co-assembly of blood and cell favourable/bioactive molecules with nanogels may pave the way to obtain membranes with high biocompatibility and bioactivity.<sup>47, 48</sup>

Heparin and heparin-like molecules have been intensively investigated for the modification of blood-contacting materials and tissue engineering scaffolds.<sup>48-50</sup> Different from many traditional antifouling or hemocompatible surface designs, a number of studies suggested that the heparin and heparin-like molecules immobilized surfaces showed integrated diminished thrombogenic response and remarkable blood and cell compatibility.<sup>10, 25, 51</sup> Meanwhile, the heparin and heparin-like

molecules exhibited significant ability on the angiogenesis while reducing the need for exogenous growth factors in *in vivo* studies.<sup>48, 52</sup> However, being an animal-derived product, the utilization of heparin in surface systems might have potential side effects (e.g., immune reactions, human growth factors and enzymes interference). Taking heparin-like molecules to design heparin-mimicking surface may present high impacts for the advancement of modified multifunctional biomedical membranes.

In this study, a novel 3D multifunctional layer was fabricated on a typical biomedical membrane surface by using LBL self-assembly of nanogels and heparin-mimicking polymers. To integrate long-term antibacterial activity, Ag NPs embedded nanogels were firstly prepared. As one of the most important clinical used artificial membranes, polyethersulfone (PES) membrane was chosen as the substrate for surface nanosystem construction. The typical self-assembly of the Ag-nanogels on the membrane surface was prepared by using an electrostatic LBL method. To obtain heparin-mimicking surface, the as-prepared nanogel coated membranes were further assembled with a typical heparin-like polymer, poly(styrenesulfonate) (PSS), by two different processes. The surface chemical components of the modified surfaces were characterized through fourier transform infrared spectroscopy (FTIR) and X-ray photoelectron spectroscopy (XPS); the 3D morphology of nanogels assembled surfaces were observed by scanning electron microscopy (SEM) and atomic force microscopy (AFM). The blood compatibility and antithrombotic property of the modified membrane surfaces were evaluated in terms of water contact angle (WCA), bovine serum albumin (BSA) adsorption, bovine fibrinogen (BFG) adsorption, anticoagulant times, and anti-platelet adhesion. The endothelial cells morphology observation was taken to demonstrate the cell-biointerface interaction and cell toxicity of the obtained heparin-mimicking membranes. The antibacterial activities of these Ag-nanogel assembled membranes were carried out by using *Escherichia coli* and *Staphylococcus aureus* bacteria.

## 2. Experimental

### 2.1 Materials

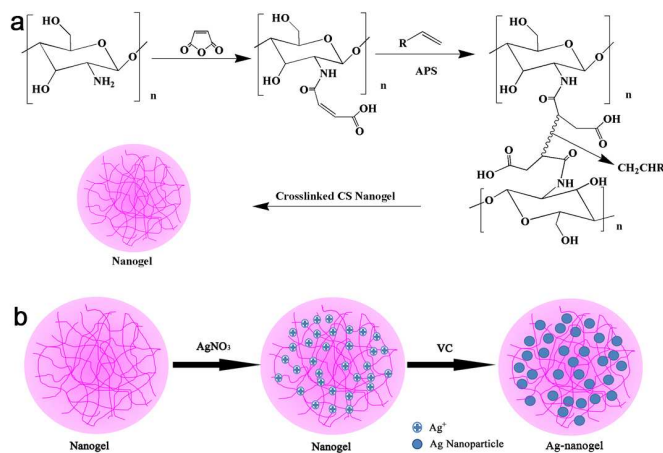
Chitosan (CS, viscosity: 100-200 mPa.s, deacetylation degree of 95%, Aladdin). N,N'-Methylidenebis(acrylamide) (MBA), ammonium persulfate (APS), maleic anhydride (MA), N-Isopropylacrylamide (NIPAM), and silver nitrate (AgNO<sub>3</sub>) were purchased from Aladdin reagent Co. Ltd. (China). Polyetherimide (PEI, average Mw: 100000) and poly (sodium 4-vinylbenzenesulfonate) (PSS, average Mw: 100000) were purchased from Sigma Aldrich. Bovine serum albumin (BSA, fraction V, 95%) bovine fibrinogen (BFG, fraction V, 95%) was obtained from Sigma Aldrich. Micro BCA™ Protein Assay Reagent kits were the products of PIERCE. Phosphate-buffered saline (PBS, pH = 7.2-7.4) solution is used to dissolve BSA. 3-(4, 5-dimethylthiazol-2-yl)-2, 5-diphenyl tetrazolium bromide (MTT) reagent was purchased from Sigma Aldrich. Beef extract and calf serums were of analytical grade and purchased from Kebite bio-reagent, Chengdu. Other reagents were obtained from Aladdin reagent Co. Ltd. (China) with analytical grade and used as received unless otherwise stated. All the aqueous solutions were prepared with de-ionized water (DI water). Dialysis membranes (MWCO = 8000-14000 Da) were obtained from Solarbio (Canada). Polyethersulfone (PES, Ultrason E6020P, BASF) were used as received. The

homemade PES UF membranes were prepared as described in our earlier paper.<sup>28</sup>

## 2.2 Preparation of nanogels and Ag-nanogels

In this study, we take the advantages of the designed 3D surface assembly and the multifunctionality of nanogels. The nanogels were prepared by a typical in-situ cross-linked polymerization of allyl components consisting of NIPAM and allylate CS derivative, where the CS derivative was used as stabilizer as well as for the further binding of Ag ions. For the design of antibacterial biointerfaces for a long-term implantation, the nanogels were subsequently employed as templates for the loading of Ag nanoparticles by in situ binding of Ag ions within the nanogel networks through ionizable carboxyl acid groups, and then reduced with vitamin C (VC).

The preparation of the nanogels is similar to an earlier report with a minor modification, and a typical surfactant-free in-situ self-crosslinking method by free radical polymerization was used, as shown in Scheme 1. Before the self-crosslinking, vinyl groups are anchored onto the CS backbone firstly by the introduction of MA: 5.32 g CS and 11.6 g MA were added to 270 mL formic acid; and the reaction was carried out at 55 °C for 12 h. Then, the allylate CS derivative polymer was precipitated in isopropyl alcohol. The allylate CS derivative was washed by acetone and dried in vacuum. To confirm the successful synthesis of the allylate CS derivative, fourier transform infrared spectroscopy (FTIR) spectra (Nicolet 560, American) and <sup>1</sup>H-NMR data (Bruker AVII-400 MHz spectrometer, Germany; DMSO-d<sub>6</sub> was used as the solvent) were collected.



**Scheme 1** (a) Synthesis process of nanogels and the chemical structures. (b) Synthesis process of Ag-nanogel.

After that the MA grafted CS was obtained, nanogel particles were synthesized by a surfactant-free emulsion polymerization as described in following: typically, 1 mL MA grafted CS solution (3 wt. %, in formic acid/water 3:7 v/v), 210 mg NIPAM, 5 mg MBA and 6 mL DI water were mixed together. Nitrogen was bubbled through for 15 min to remove the dissolved oxygen. After being stabilized for 30 min at 70 °C, the emulsion polymerization was initiated by adding 90 μL APS (10 wt. %) and carried out at 70 °C for 6 h. Then the obtained nanogels were purified via dialysis against DI water for 1 week to remove the monomers and any other residues.

In a typical procedure for the preparation of Ag-nanogels, 8 mL of the above obtained nanogel solution was placed into a

30 mL flask. The pH value of the solution was adjusted to 8.8 by adding 0.1 M NaOH and the total volume of the solution was controlled to 18 mL, and then 3 mL 0.1 M AgNO<sub>3</sub> was added. After stirring for 5 h in the dark, the solution was dialyzed against DI water for 2 d to remove the excess of AgNO<sub>3</sub>. Then, the solution was heated to boiling, and then 1 mL of 0.075 M VC in DI water was added to reduce the Ag ions into Ag nanoparticles. The reaction was continued for 1 h at 100 °C; finally, the hybrid particles were purified by dialysis in DI water. The Ag loaded hybrid particles are termed Ag-nanogels and the synthesis process is shown in Scheme 1b.

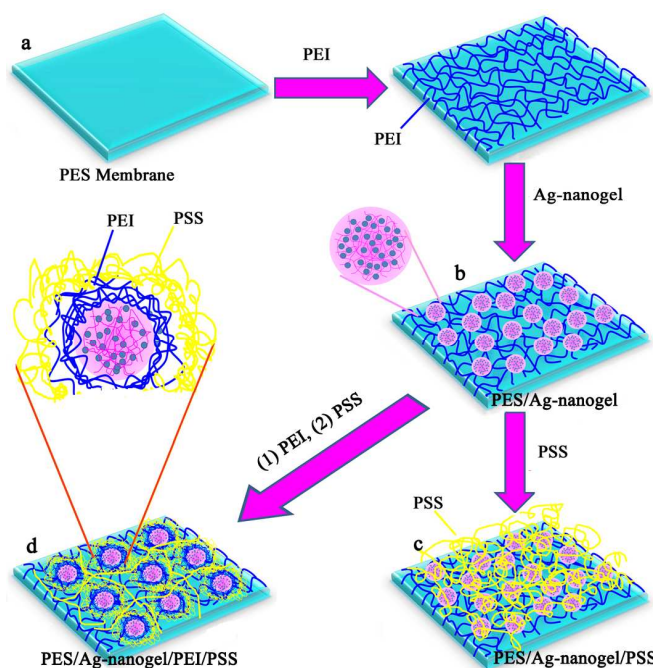
## 2.3 3D surface nanogels assembly onto PES substrates

Prior to 3D surface nanogels assembly, homemade polyethersulfone (PES) membranes were prepared as indicated in our earlier report.<sup>28</sup> The surface assembly started with a typical surface treatment by immersing the membranes in positively charged PEI (10 mg/ml) solution for 12 h at 25 °C, and the rotation speed was 150 r/min; then the membranes were rinsed with DI water for 3 times to remove the unstable PEI. The 3D surface nanogel assembly was carried out by immersing the membranes into the solution of negatively charged Ag-nanogels (about 10 mg/mL) for 10 min. To obtain heparin-mimicking surface, the as-prepared nanogel coated membranes were further assembled with a typical heparin-like polymer, PSS, by two different processes. For the first one, the PES/Ag-nanogel membrane was directly immersed in the PSS solution (10 mg/ml) to obtain PES/Ag-nanogel/PSS membrane; for the second one, the PES/Ag-nanogel membrane was sequentially immersed in the PEI (10 mg/ml) and PSS (10 mg/ml) solutions to obtain PES/Ag-nanogel/PEI/PSS membrane (after PEI immersion, the membrane was also rinsed with DI water). All the exposure times for each assembly were 10 min, respectively. After each layer deposition, the sample was repeatedly immersed in DI water 3 times for about 5 min to remove the excess assembling materials, and then the functionalized membranes were dried with nitrogen.

## 2.4 Construction of the 3D nanogel assembled and functionalized membranes

In this study, the facile and green LBL assembly approach was proposed to prepare surface 3D nanogel assembled membranes as indicated in Scheme 2. Briefly, the surface assembly process started with a typical surface treatment by immersing the membranes in positively charged PEI solution, which could anchor onto the PES membrane and confer the positively charges for further LBL assembly. The 3D surface nanogel assembled membranes (PES/Ag-nanogel) were fabricated by immersing the membranes into the negatively charged Ag-nanogel solution. Then, to obtain heparin-mimicking surface, the PES/Ag-nanogel membranes were further assembled using a typical used heparin-like polymer, PSS, by two different processes. For the first process, the PES/Ag-nanogel membrane was directly dipped into the PSS solution to obtain PES/Ag-nanogel/PSS membrane as shown in Scheme 2b; for the second one, the PES/Ag-nanogel membrane was sequentially immersed in the PEI and PSS solution to obtain PES/Ag-nanogel/PEI/PSS

membrane as shown in Scheme 2c; meanwhile, the processes might be accompanied with morphology change of Ag-nanogel which will be discussed in section 3.2.2. The assembly mechanism should be resulted from the electrostatic interaction and the adhesive ability of the polyelectrolyte.



**Scheme 2** The fabrication processes for the 3D nanogel deposited membranes by surface engineered LBL assembly. (a) pristine PES membrane, (b) PES/Ag-nanogel, (c) PES/Ag-nanogel/PSS, and (d) PES/Ag-nanogel/PEI/PSS.

Membrane surface Zeta-potentials of (with were measured using a Beckman Coulter, Delsa™ NanoC Analyzer with a membrane test vessel (membrane testing model with an area of  $1 \times 3 \text{ cm}^2$ ) at  $37^\circ \text{C}$ .

### 2.5 *In-vitro* blood compatibility tests

The membrane hydrophilicity was characterized via the data of static water contact angle. Detailed methods are shown in supporting information.

Protein adsorption experiments were carried out with BSA solutions and BFG solution under the static condition, respectively. The protein concentration in the washing solution was used to calculate the adsorbed protein amounts and determined by using the Micro BCA™ Protein Assay Reagent Kit (PIERCE). Detailed methods are shown in supporting information.

To evaluate the antithrombotic activity of the heparin-mimicking membranes, activated partial thromboplastin time (APTT) and thrombin time (TT) were measured to evaluate the blood clotting time and thrombotic potential.<sup>28</sup> Detailed methods are shown in supporting information.

For the anti-platelet adhesion tests, the platelet-rich-plasma (PRP) was used for the study of platelet adhesion on the nanogels and heparin-like polymers assembled membranes

using healthy fresh human blood.<sup>53</sup> Detailed methods are shown in supporting information.

### 2.6 *In-vitro* Cell compatibility measurements

Human umbilical vein endothelial cells (HUVECs) were applied to exam the cell compatibility of the modified membranes. Cells were cultured in R1640 medium, which was supplemented with 10% fetal bovine serum (FBS, Hyclone, USA) and 2 mM L-glutamine and 1% (*V/V*) antibiotics mixture (10000 U penicillin and 10 mg streptomycin). The cell morphology on the membranes was examined by a FE-SEM (JSM-7500F, JEOL, Japan) via sputter-coated with a gold layer. Detailed methods are shown in supporting information.

### 2.7 Antibacterial activity tests

*Escherichia coli* (*E. coli*, gram-negative) and *Staphylococcus aureus* (*S. aureus*, gram-positive) bacteria were used as the model bacteria to evaluate the antibacterial characteristics and bactericidal efficacy of the Ag-nanogels assembled membranes. The samples were also with an area of  $1 \times 1 \text{ cm}^2$ , before the microbiological experiment, all the glasswares and the samples were sterilized by ultraviolet radiation for 30 min.

The antibacterial capability of the Ag-nanogel assembled membrane was firstly investigated by an inhibition zone method. The sterilized membranes were placed on *E. coli*, and *S. aureus* bacteria agar plates at an inoculum concentration of  $10^6$  colony forming units per ml (cfu/mL), respectively; and then incubated at  $37^\circ \text{C}$  for 24 h. At the concentration of  $10^6$  cfu/mL, the presence of the inhibition zone was monitored and recorded by a digital camera.

The concentrations of *E. coli* and *S. aureus* at  $10^6$  cfu/mL were also used for antibacterial test using colony forming count method. The samples were immersed in 2 mL of bacterial suspension and incubated in a shaking incubator at  $37^\circ \text{C}$  for 12 h. Then the optical degree of the bacterial suspension was calculated by UV-vis absorbance.

For the evaluation of the antibacterial adhesion characteristics and bactericidal efficacy for the surface assembled membranes, the bacteria were suspended at a concentration of  $10^6$  cfu/mL, and the substrate was immersed in 2 mL of the bacterial suspension under static condition at  $37^\circ \text{C}$  for 24 h. The adhered bacterial cells were observed under a scanning electron microscope after fixing with 2.5 % glutaraldehyde and dehydration with serial ethanol similar to the HUVECs observation as mentioned above.

## 3. Results and discussion

### 3.1 Characterization of nanogel and Ag-nanogel

Figure 1a and b show the FTIR spectra for the pristine CS and the MA grafted CS. The absorption peaks at 1616 and  $1099 \text{ cm}^{-1}$  in Figure 1a are attributed to the carbonyl stretching vibration (amide I) and the C–O–C stretching vibration of the ether linkage in CS backbone, respectively. For the spectrum of MA grafted CS, as shown in Figure 1b, besides the characteristic absorption bands of CS at 1616 and  $1099 \text{ cm}^{-1}$ ,

the MA grafted CS shows a new peak at  $1721\text{ cm}^{-1}$  which is assigned to the carboxyl group (derived from the MA). Thus, the FTIR spectra indicate that the MA has been grafted onto the CS successfully. Figure 1c and d show the  $^1\text{H-NMR}$  spectra for the CS and the MA grafted CS, the chemical shifts at  $\delta=11.432$  ppm (Figure 1c) and  $\delta=2.506$  ppm (Figure 1d) are attributed to the solvents ( $\text{CF}_3\text{COOD}$  and  $\text{DMSO-d}_6$ ), respectively. The chemical shift at  $\delta=6.043$  ppm (Figure 1d) is attributed to the  $\text{RCH=CHR}$  group of the MA, which confirmed the successful grafting.

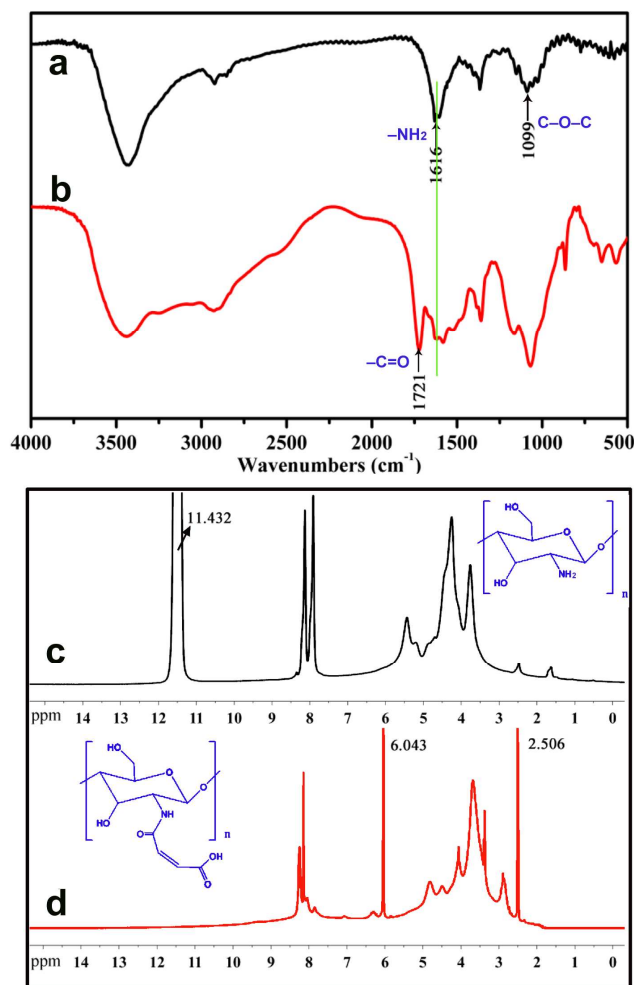


**Figure 1** FTIR spectra for (a) CS and (b) MA grafted CS;  $^1\text{H-NMR}$  spectra for (c) CS dissolved in  $\text{CF}_3\text{COOD}$ , (d) MA grafted CS dissolved in  $\text{DMSO-d}_6$ .

The morphologies of the as-prepared Ag-nanogels are observed by Transmission Electron Microscopy (TEM) as shown in Figure 2a, the synthesized nanogels (about  $110\pm 20$  nm) were well dispersed with round shape, which indicated that the strategy might be apply to large scale production. The loaded AgNPs presented well distributed size ranging from about 5 nm to 15 nm. The chemical components and the purity of the CS based nanogels and Ag-nanogels were investigated by XRD patterns. Figure 2b displays the X-ray Diffraction (XRD) patterns, the characterized peak of the nanogel appeared at  $24.6^\circ$ , corresponding to the characteristic peak of the cross-linked polymers. The presence of AgNPs in the nanogel was further confirmed by XRD, and the diffraction peaks appeared

at  $38.5^\circ$ ,  $44.8^\circ$ ,  $64.7^\circ$ ,  $77.8^\circ$  and  $82.1^\circ$ , which were assigned to the (111), (200), (220), (311) and (222) crystalline planes of Ag, respectively.

The UV-vis reflectance spectra of the nanogels and Ag-nanogels are shown in Figure 2c. Compared with the UV-vis reflectance spectra of the nanogels, the spectra of Ag-nanogel solution showed an obvious absorption band at 418 nm, which further confirmed the presence of the silver in the sample. As shown in the inserted columnar image of Figure 2c, the diameter of the Ag-nanogel particles mainly ranged from 90-210 nm, the average diameter is 156 nm, and the polydispersity index (PDI) is 0.344, and the zeta potential was about  $-8.68$  mV for the Ag-nanogels.

The thermal stabilities and the detailed Ag contents of the hybrid nanogels were analyzed by thermo-gravimetric analysis (TGA) in air atmosphere with a heating rate of  $10\text{ }^\circ\text{C}/\text{min}$ , as shown in Figure 2d. For the two kinds of nanogels, the degradation can be divided into two steps. Firstly, there are about 10 % weight loss for the Ag-nanogels and 15 % weight loss for nanogels around  $100\text{ }^\circ\text{C}$ , which was related to the destruction of the bonded water molecules in the nanogels. Secondly, there was one sharp weight loss in the range of  $200\text{ }^\circ\text{C}$ - $568\text{ }^\circ\text{C}$ , at which the nanogels lost its weight by 85 wt. % and retained 0 wt. % at last. Compared to the CS based nanogels, the Ag-nanogel retained as high as 15 wt. %, which indicated that the Ag-nanogels comprised 85 wt. % polymers and 15 wt. % Ag NPs. These results confirmed the successfully in situ growth of Ag NPs; and the high loading ratio of the Ag NPs indicated that the as-prepared Ag-nanogel might exhibit efficient antibacterial ability.

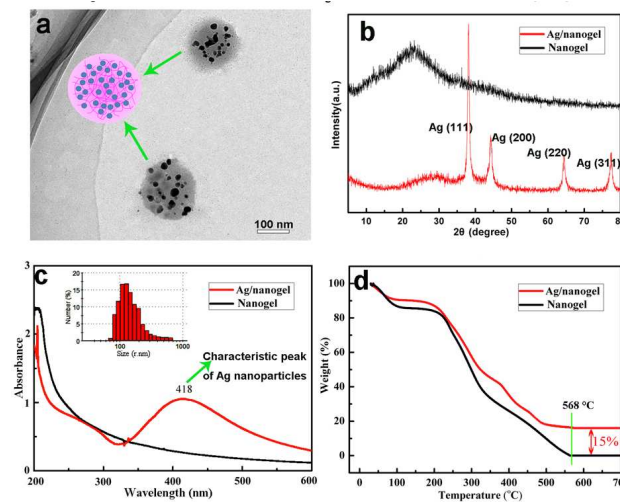


**Figure 2** (a) TEM image of the Ag-nanogels. (b) XRD patterns of the nanogels and the Ag-nanogels. (c) The UV absorbance of the nanogels and Ag-nanogels, the inserted columnar image presents the size distribution of the obtained Ag-nanogels. (d) TGA curves of the nanogels and Ag-nanogels, the test condition is  $10\text{ }^\circ\text{C}/\text{min}$  in air.

### 3.2 Characterization of 3D nanogel assembled and functionalized membranes

Field emission scanning electron microscope (FE-SEM) images of the samples were obtained by a scanning electron microscope (FEI Sirion-200, USA). Atomic force microscopy (AFM) images of the samples were acquired using a Multimode Nanoscope V scanning probe microscopy (SPM) system

(Veeco Instruments Co., USA). The surface chemical structures and compositions of the coated PES membranes were characterized by Attenuated total reflection-Fourier transform infrared spectra (ATR-FTIR) (Nicolet 560, America) and X-ray Photoelectron Spectroscopy (XPS; KRATOS, AXIS Ultra DLD, Britain) instrument.

The surface chemical compositions of the membranes were analyzed by ATR-FTIR spectroscopy and XPS. As shown in Figure 3a, there were barely any obvious peaks above  $1600\text{ cm}^{-1}$  for the pristine PES membrane. After the surface assembly of the Ag-nanogels, a new broad peak at  $1665\text{ cm}^{-1}$  appeared, which was attributed to the overlapped peaks of the bending vibrations of the N-H and  $\text{-C=O}$ .<sup>54</sup> Meanwhile, for the PSS coated membranes, the characteristic peaks of PSS were observed: the peaks at  $1038\text{ cm}^{-1}$  and at  $1008\text{ cm}^{-1}$  were ascribed to the symmetric stretching vibrations and the asymmetrical stretching vibrations of the high polar  $\text{-SO}_3^-$  groups of PSS brushes, respectively.<sup>28</sup> The results of the characteristic peaks indicated that the Ag-nanogels and the PSS polymers had been coated onto the PES membrane surfaces; the intensive  $\text{-SO}_3^-$  group characteristic peaks of the PES/Ag-nanogel/PEI/PSS indicated higher PSS coating amount than that of the PES/Ag-nanogel/PSS.

In order to confirm the enrichment amount of the Ag-nanogels and PSS coating layer on the membrane surface in detail, XPS wide spectra was employed to characterize the surface chemical compositions for the PES and Ag-nanogel assembled PES membranes, as shown in Figure 3b. For the pristine PES membrane, no peaks of N and Ag elements were observed. While, for the PES/Ag-nanogel membrane, the peaks of N and Ag elements emerged and the peak intensity of the S element decreased dramatically, which indicated that the PES surface were completely covered by the Ag-nanogels. Meanwhile, the PES/Ag-nanogel/PEI/PSS showed evidently higher S element peak intensity, indicating higher PSS coating amount than that of the PES/Ag-nanogel/PSS. The FTIR and XPS data indicated that the PSS coated layer was very thick for the PES/Ag-nanogel/PEI/PSS membrane, which may influence the membrane surface morphology.

The surface morphology is an important parameter for biomedical membrane, which may affect the interface energy and also the interaction between the bio-components and the material surfaces. To gain further information and understand the microstructures of the Ag-nanogel coated membrane surfaces, SEM and AFM observations were carried out and the results are shown in Figure 4 and Figure 5.

Field-emission SEM images with different magnifications are presented in Figure 4 for the detection of the surface morphologies. It was observed that the pristine PES membrane surface exhibited a relative smooth 2D structure, and no obvious pores or particles are observed. However, for the Ag-nanogel assembled membranes as shown in Figure 4b, numerous well distributed nanogels were observed, ranging from  $100\text{ nm}$  to  $200\text{ nm}$ . The results indicated that the assembled nanolayer composed of Ag-nanogels, and the sizes of the assembled nanogels were coincident with the results as shown in Figure 2e. Furthermore, the EDS spectrum (Figure 4e) acquired for the PES/Ag-nanogel membrane clearly demonstrates the existence of the Ag NPs. For the PES/Ag-nanogel/PSS membrane, as shown in Figure 4c, it was hard to detect the thin layer of heparin-mimicking polymer (PSS); while, the assembled surface became smoother than the PES/Ag-nanogel, combined with the FTIR and XPS data, it can be concluded that the PSS layer had assembled onto the membrane surface. For the PES/Ag-nanogel/PEI/PSS, as shown in Figure 4d, the morphology and size of the assembled nanogels were much larger than the pristine Ag-nanogel with the size ranged from  $200\text{-}450\text{ nm}$ ; meanwhile, typical random assembled polymer layers were also observed due to the assembly of the abundant positive (PEI) or negative (PSS) polymers. It was suggested that the PEI and PSS resulted in the Ag-nanogel morphology change during the assembly process. PEI chains exhibited strong adhesive ability with the Ag-nanogel, and then might tightly enwrap with the Ag-nanogel and transferred the negatively charged Ag-nanogels to positively charged nanogels; thus, during the further assembly of the heparin-mimicking polymer (PSS), the PSS chains would also tightly enwrap around the PEI coated Ag-nanogels and led the coated nanogels become much larger than the pristine Ag-nanogels.

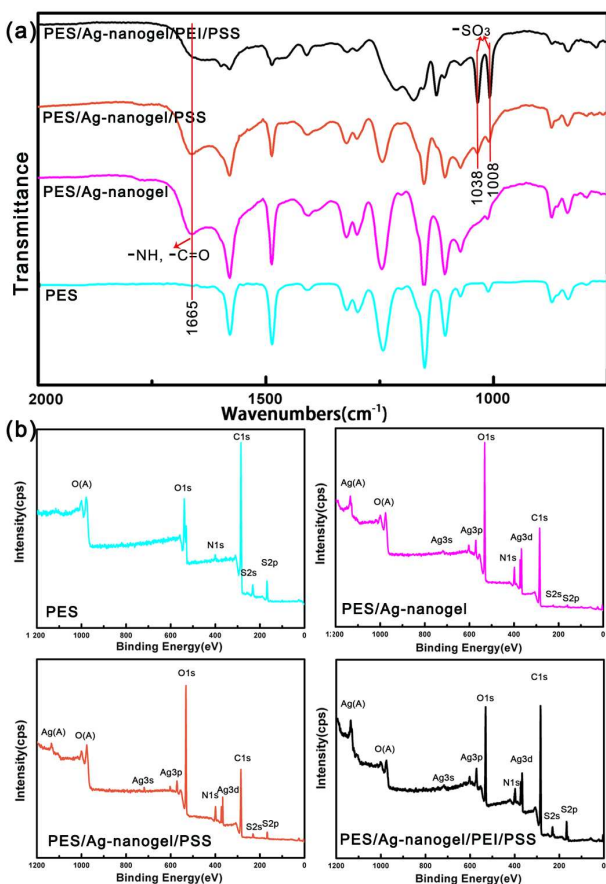


**Figure 3** (a) ATR-FTIR spectra and (b) XPS patterns for PES, PES/Ag-nanogel, PES/Ag-nanogel/PSS, PES/Ag-nanogel/PEI/PSS.

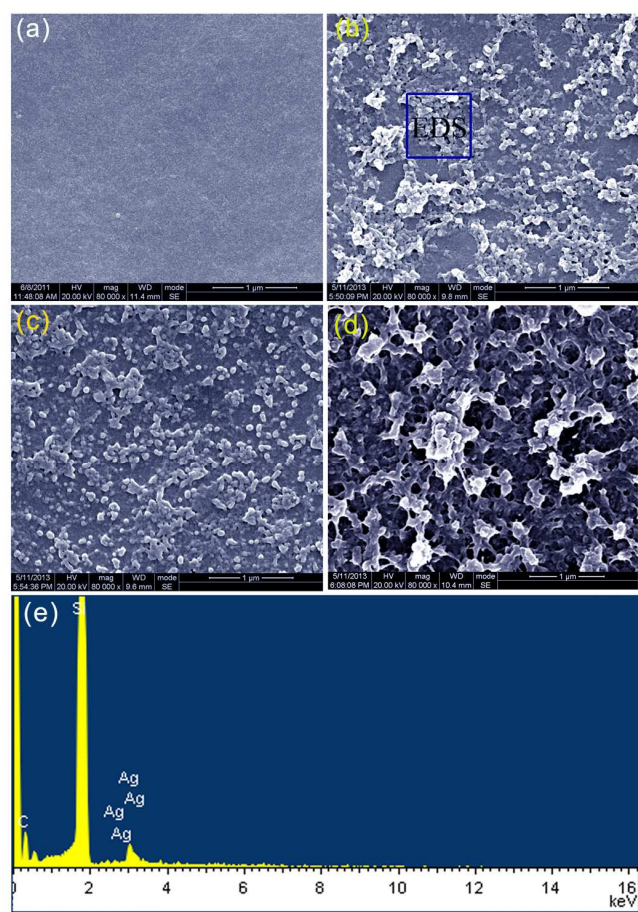


**Figure 4** Surface SEM images for the (a) PES, (b) PES/Ag-nanogel, (c) PES/Ag-nanogel/PSS, (d) PES/Ag-nanogel/PEI/PSS, and (e) surface EDS spectrum. For a, b, c and d the scale bar is 1  $\mu\text{m}$ .

As one of the most appropriate methods for definitive identification of materials surface, the 2D and 3D AFM image analysis was carried out for further investigation of the surface morphology change of the Ag-nanogel assembled membranes. As presented in Figure 5, the typical 10  $\mu\text{m}$  scan images for the PES membrane and the Ag-nanogel assembled membranes were taken. The AFM image of pristine PES membrane clearly verified the characteristic 2D flat membrane. While, after the Ag-nanogel assembly, it was observed that the surface morphology of the PES/Ag-nanogel membranes became rougher and there were a lot well distributed Ag-nanogels, which was coincident with the results of FE-SEM images. Moreover, the PES/Ag-nanogel/PEI/PSS membrane presented a much rougher surface morphology with larger assembled nanogels than that of the PES/Ag-nanogel membrane as indicated in the FE-SEM images.

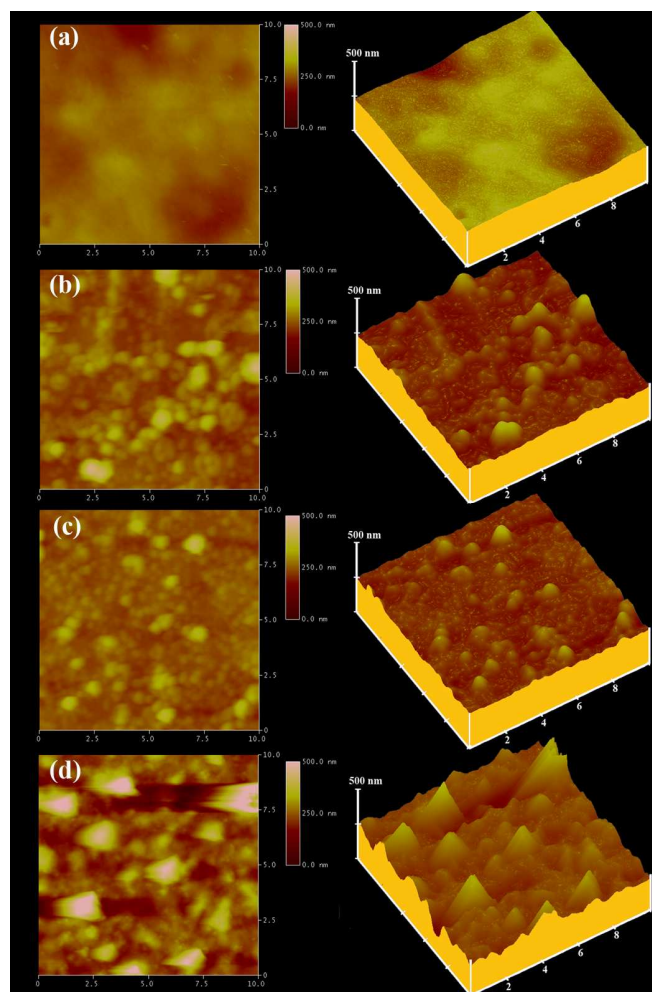


**Figure 5** Surface AFM images for the (a) PES, (b) PES/Ag-nanogel, (c) PES/Ag-nanogel/PSS, and (d) PES/Ag-nanogel/PEI/PSS membranes. The scale bars of X and Y axes are 10  $\mu\text{m}$ .

### 3.3 Blood compatibility

For the design of advanced blood-contacting biomedical membranes, the blood compatibility, such as plasma protein adsorption, anticoagulant ability, and anti-platelet adhesion to the biointerfaces, is the priority and essential event that needs to be well evaluated.

The zeta potential for PES membrane was  $-5.51$  mV; while, the PEI adhered PES substrate increased to  $+20.08$  mV. For the PES/Ag-nanogel membrane, the zeta potential decreased to  $+4.53$  mV after the assembly of Ag-nanogel. PSS assembled membranes exhibited a negatively charged surface, the Zeta potential of PES/Ag-nanogel/PSS membrane is  $-18.50$  mV, and the PES/Ag-nanogel/PEI/PSS membrane is  $-25.60$  mV.

The surface hydrophilic/hydrophobic property plays important role in material-associated blood compatibility; the hydrophobic surface may result in serious plasma component adsorption, especially the protein adsorption and clotting enzymes. Thus, the integrated hydrophilicity is highly desired for the improvement of blood compatibility. The water contact angle is the most convenient parameter to assess the hydrophilic/hydrophobic property of membrane surface, which provides information on the interaction energy between the surface and liquid. The hydrophilicity of the nanogel assembled

membrane surface was characterized by using static contact angle measurement as shown in Figure 6a. The pristine PES membrane presented a high contact angle of about  $79^\circ$ , corresponding to low surface hydrophilicity. After coating the Ag-nanogels, the contact angles decreased dramatically (PES/Ag-nanogel ( $22^\circ$ ), PES/Ag-nanogel/PSS ( $35^\circ$ ), PES/Ag-nanogel/PEI/PSS) ( $32^\circ$ ), which indicated that the modified membranes became more hydrophilic with the coating of the nanogels onto the surfaces. The relatively low contact angle of the PES/Ag-nanogel may be resulted from the capillarity between the porous morphology of the nanogels.

Intensive plasma protein adsorption on material surfaces is the first matter that needs to be concerned for the blood-contacting biomedical materials.<sup>54</sup> The amount of protein adsorbed on material surface is considered to be one of the important factors in evaluating the blood compatibility of materials.<sup>55</sup> It has been reported that materials possessed low protein adsorption might own improved blood compatibility.

In the present work, the surfaces of the membranes were studied in relation to the adsorption of BSA and BFG in vitro, since BSA and BFG are the most typical plasma proteins which might present direct connection with the blood compatibility. Figure 6b shows the adsorbed amounts of BSA and BFG protein on the membrane surfaces. It was found that all the Ag-nanogel assembled membranes exhibited much lower BSA and BFG adsorption amounts than that of the pristine PES membrane. The PES/Ag-nanogel membrane achieved the lowest value of about  $2 \mu\text{g}/\text{cm}^2$ , which was much better than the commercial used PES dialysis membrane. The decreased protein adsorption could be attributed to the highest hydrophilicity of the PES/Ag-nanogel membrane as indicated in the water contact angle.<sup>56</sup> While, the PES/Ag-nanogel/PSS and PES/Ag-nanogel/PEI/PSS membranes achieved lower BFG adsorption amounts than the PES/Ag-nanogel membrane, which may be resulted from the negatively charged heparin-mimicking surface design. It has been reported that materials owned hydrophilic or negatively charged surfaces could decrease nonspecific protein adsorption. Therefore, the coated PES membranes had lower BSA and BFG adsorption amounts than those for the pristine PES membrane. Meanwhile, it was found that the PES/Ag-nanogel/PSS and PES/Ag-nanogel/PEI/PSS membranes owned lower BFG adsorption amount; thus it was expected that the PES/Ag-nanogel/PSS and PES/Ag-nanogel/PEI/PSS membranes might perform better anti-platelet adhesion, since fibrinogen (indicated by BFG) in blood plasma was particularly important for platelet adhesion, which could bind to platelet GP IIb/IIIa receptor.

During clinical hemo-contacting applications, anticoagulant reagent, such as heparin, is needed to prevent the occurrence of thrombus or blood coagulant; however, the use of anticoagulant reagent might exhibit great influence on human being since the anticoagulant reagent could flow into other organs and tissues and react with a wide of blood and tissues components. Thus, self-anticoagulant membranes are highly demanded during these applications. When the anticoagulant reagent was integrated onto the surface of biomedical dialysis membranes, it might only combine or react with coagulation factors and exhibit limited effect on the other blood and tissues components. Recently, inspired from the biological blood and cell compatibility of heparin, heparin-like polymers were designed and used to improve the biocompatibility of biomedical materials by mimicking the structure of heparin via the introduction of functional groups, such as sulfonic or carboxylic acid group contained polymers. One goal of this

study is to design heparin-mimicking surface with specific anticoagulant property to enable the Ag-nanogel assembled membranes satisfy various clinical biomedical applications.

Thus, the biological anticoagulant activity of the heparin-mimicking polymer (PSS) assembled PES/Ag-nanogel membranes was further investigated by using activated partial thromboplastin time (APTT) and thrombin time (TT) tests. In general, APTT was used to measure the inhibited efficacy both of the intrinsic (or referred to as the contact activation pathway) and the common plasma coagulation pathways including factors II, V, X, XII or fibrinogen. TT was used to measure the clot formation time taken for the thrombin converted fibrinogen into fibrin in platelet-poor plasma (PPP). The shorter clotting time indicated the faster conversion of fibrinogen into insoluble fibrin protein, which then can lead to thrombus.<sup>57</sup>

The APTT and TT for the pristine PES membrane and the functionalized PES membranes were measured, data are shown in Figure 6c, and the results were analyzed by statistical methods (significant difference,  $P < 0.05$ ). For the functionalized membranes, the APTT increased gradually compared with the pristine PES membrane ( $*P < 0.05$ ); The APTT for PES/Ag-nanogel/PEI/PSS membrane presented the longest blood clotting time due to the highest PSS content, which was more than 1.5 times than that for the pristine PES membrane. The TT tests also showed that the clotting time of the heparin-mimicking surface was prolonged.

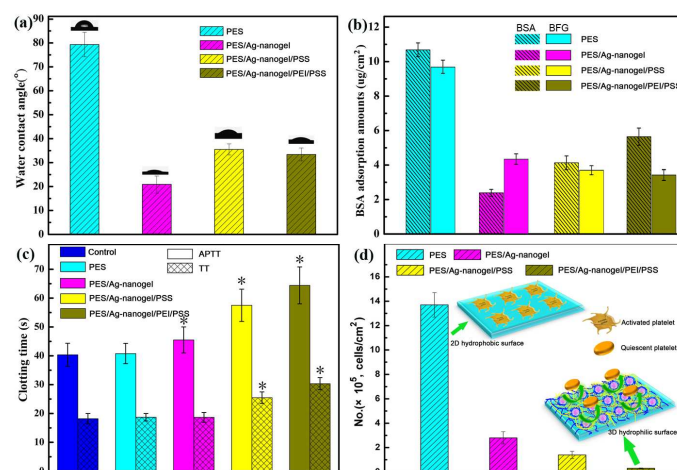


**Figure 6** (a) The water contact angles of the PES membrane and 3D surface nanogels assembled membranes. The results were expressed as means  $\pm$  SD ( $n = 8$ ). (b) Protein adsorbed amounts of pristine PES and 3D surface nanogels assembled membranes, the BSA and BFG adsorptions were measured in separate experiment. The results were expressed as means  $\pm$  SD ( $n = 3$ ). (c) The APTT and TT clotting times for the pristine PES and heparin-mimicking membranes. For the control group, 5  $\mu\text{L}$  PBS was added instead. Values are expressed as means  $\pm$  SD ( $n = 3$ ). The marks (\*) meant that the difference attained a statistically significant increase compared with the control.  $*P < 0.05$ . (d) The average number of the adhering platelets onto the membranes from platelet-rich plasma estimated by 6 SEM images.

For blood-contacting materials, the adhesion of platelets to the biointerfaces is the key response before the thrombus formation.<sup>58</sup> The activated platelets may accelerate thrombosis and then led further coagulations. Thus, in this study, the adhered platelet number and the morphologies of the adhered platelets were investigated to evaluate the blood compatibility of the heparin-mimicking membranes.

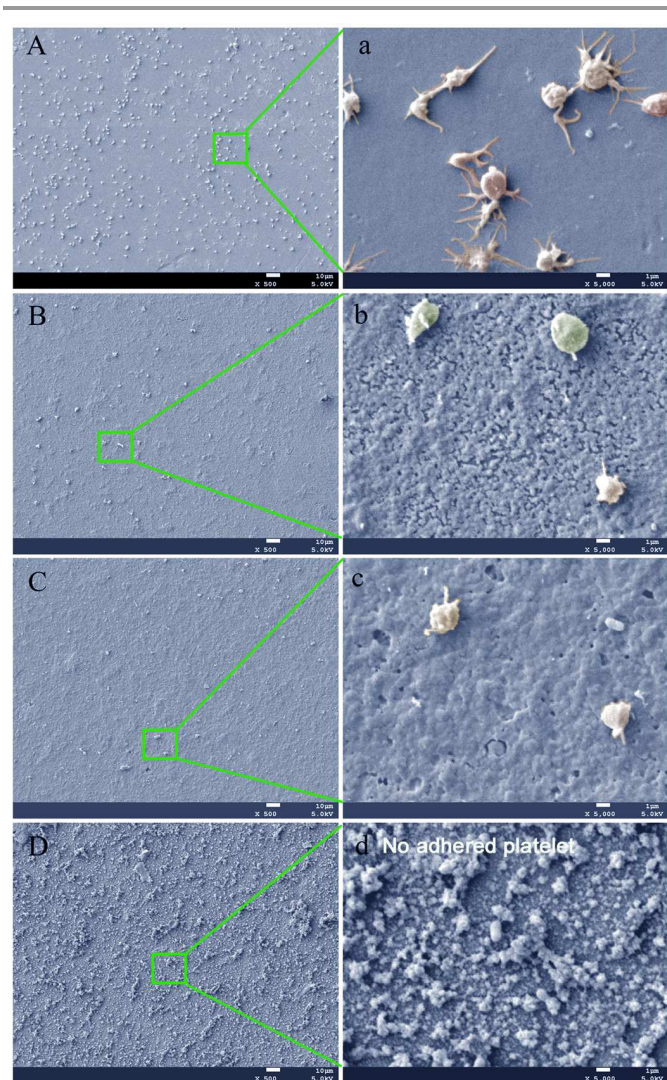


**Figure 7** SEM images of the surface adhered platelets of the (A, a) PES, (B, b) PES/Ag-nanogel, (C, c) PES/Ag-nanogel/PSS, and (D, d) PES/Ag-nanogel/PEI/PSS membranes. The scale bars are 10  $\mu\text{m}$  (left) and 1  $\mu\text{m}$  (right).

As indicated in Figure 6d, the average numbers of the adhered platelets decreased significantly for the surface Ag-nanogel assembled membranes compared to the pristine PES substrate. The suppressed platelet adhesion was attributed to the improved hydrophilicity and the negative charges due to the assembly of the Ag-nanogels and PSS polymer layer. Meanwhile, it was striking to find that the adhered platelet decreased dramatically with the increase of the PSS amount, and there was almost no platelet adhered onto the PES/Ag-nanogel/PEI/PSS even though the membrane owned 3D rough surface morphology as indicated in Figure 7. As shown in the typical SEM images of the platelet adhering membranes, it was observed that numerous platelets were aggregated and accumulated on the PES membrane surface; these platelets spread in flattened and irregular shapes, and abundant pseudopodia were observed. However, for the Ag-nanogel and PSS assembled membranes, the adhered platelets were rarely observed; and the platelets expressed rounded morphology. This should be attributed to the increased hydrophilicity and relatively low BSA and BFG adsorption on the functionalized membranes. The earlier reports indicated that the rougher

surface was favorable to the adhesion of platelet; however, in this study, the highly rough PES/Ag-nanogel/PEI/PSS membrane surface exhibited ultralow platelet adhering amount than the other membranes. Therefore, except from the hydrophilicity and low protein adsorption, the large amount of the highly coated negative charged PSS onto the heparin-mimicking membranes are suggested to be responsible for the anti-platelet adherence due to the electrostatic repulsion and the low fibrinogen adsorption (indicated by BFG, which is particularly important for platelet adhesion). In general, both the outspread and pseudopodium deformation of the platelet were obviously suppressed for the modified membranes, which indicated that the blood compatibility of the 3D nanogel assembled and heparin-mimicking nanogel assembled PES membranes was improved.

### 3.4 Cell proliferation and viability

It is well-known that biomedical membranes have been widely employed in the fields such as artificial organs (bioartificial liver support), cell and tissue culture, and medical devices used for blood purification (like the hemodialysis, hemodiafiltration, hemofiltration, plasmapheresis and plasma collection).<sup>3</sup> Generally speaking, the cells will undergo their morphological changes to stabilize the cell-material interface after contacting biomaterials. The whole process of adhesion and spreading consists of cell attachment, filopodial growth, cytoplasmic webbing, flattening of the cell mass and the ruffling of peripheral cytoplasm progressing in a sequential fashion.<sup>59</sup> The *in vitro* cell proliferation and viability of the Ag-nanogel assembled membranes is one of the most important factors that should be carefully evaluated before the functionalized membranes can be used in biological and biomedical applications. In this study, Human umbilical vein endothelial cells (HUVECs) were selected for the evaluation of the cytocompatibility of the Ag-nanogel assembled membranes.

Figure 8 shows the typical morphology of the HUVECs cultured for 5 days on the PES and the Ag-nanogel functionalized membranes. It was observed that the HUVECs extended pseudopodia to adhere onto the materials. The amount of the HUVECs grown on the PES membrane was the least and extended with flattened morphology. For the PES/Ag-nanogel membrane, the cells spreading with ruffling of peripheral cytoplasm and extended with round shape compared with pristine PES membrane, which indicated that the assembled 3D Ag-nanogel had great influence on the cell morphology change. After the PSS coating, the cells on the PES/Ag-nanogel/PSS membrane changed to be flattened morphology and almost had covered the whole surfaces with a larger attachment area compared to the cells cultured on the PES membrane, which indicated that the heparin-mimicked PES membrane surface could promote cell attachment and growth.

Notably, the cells on the PES/Ag-nanogel/PEI/PSS membrane exhibited abundant cells spreading with ruffling of peripheral cytoplasm; moreover, as shown in Figure 8D and d, the spheroids of the HUVECs had been observed (pointed by green arrow), which were formed by the rearrangement and compaction of cell aggregates. The formation of spherical multicellular aggregates (spheroids) also had been strongly advocated as a highly useful multilayer culture mode for HUVECs instead of the traditional monolayer culture, which indicated that the 3D nanogel and heparin-like polymer assembled surface could act as tissue-like structure to promote cell proliferation and cell morphology change over a long period.<sup>60</sup>

Furthermore, the cell morphology observation also revealed the security of the silver imbedded membranes. When the materials were non-toxic, the HUVECs cells would proliferate well and cover the whole membrane. Based on the above data, it can be concluded that both the PES/Ag-nanogel/PSS and PES/Ag-nanogel/PEI/PSS membranes showed excellent cell proliferation and limited cell toxicity. While, both the pristine PES and PES/Ag-nanogel membranes exhibited relatively lower ability on cell proliferation. The cell toxicity of PES membrane should be resulted from the hydrophobic interface; as for the hydrophilic PES/Ag-nanogel membrane, the cell toxicity might be resulted from the Ag NPs, previous research has indicated that the silver NPs had some negative influence on cell growth.<sup>35</sup> However, the results demonstrated that after the introduction of heparin-like polymer, PSS, the influence of the silver NPs was greatly suppressed and the membranes exhibited good biocompatibility for endothelial cells. Thereby, we may predict that the Ag-nanogel and PSS co-functionalized membranes can maintain high cell compatibility and meantime inhibit and kill bacteria with a prolonged duration.

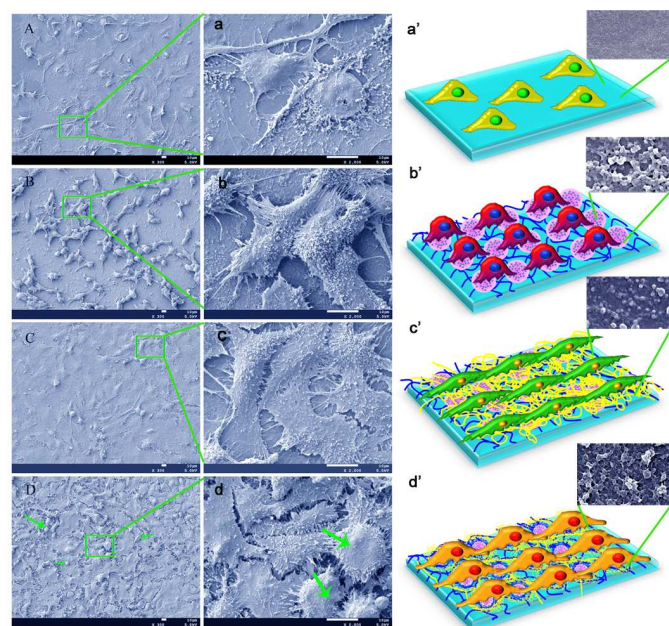


**Figure 8** SEM pictures of HUVECs cultured on the (A) PES, (B) PES/Ag-nanogel, (C) PES/Ag-nanogel/PSS, and (D) PES/Ag-nanogel/PEI/PSS after 5 days. The membranes (A, x300; a, x 2000), all the white scale bar represents 10  $\mu$ m. The spheroids were pointed by green arrow.

### 3.5 Antibacterial properties

The antibacterial activity of the multifunctional membranes was tested via bacterial inhibition zone toward *E. coli* and *S. aureus*, respectively.<sup>61</sup> As shown in Figure 9A and B, the pristine PES membrane showed no bacterial inhibition ability, while the Ag-nanogel loaded PES membranes showed significant inhibition effect on *E. coli* (Figure 9A) and *S. aureus* (Figure 9B). The sizes of inhibition zone for *E. coli* were 0.0 mm (a), 2.5 mm (b), 1.4 mm (c), and 1.0 mm (d), respectively. As for *S. aureus*, the inhibition zone is 0.0 mm (a), 5.0 mm (b), 2.0 mm (c) and 1.9 mm (d), respectively. The results indicated that the Ag-nanogel membranes had significant inhibition capacity toward both Gram-negative and the Gram-positive bacteria. As revealed by an earlier literature,<sup>46</sup> the antibacterial activity of the multifunctional membranes was mainly caused by the released  $\text{Ag}^+$  ions from the embedded silver NPs. Meanwhile, the

heparin-like polymers covered PES/Ag-nanogel membranes maintained significant inhibition zone in bacterial culture media, which confirmed that the further coating of heparin-like polymers did not interrupt the  $\text{Ag}^+$  ions release and might prolong the  $\text{Ag}^+$  ions release in culture media due to the strong binding ability of  $-\text{SO}_3^-$  group.

To confirm the antibacterial activity in aqueous solution, the optical degree of the bacterial-membranes co-cultured solution was detected. As shown in Figure 9C and D, significant bacterial growth was observed from the control sample and the pristine PES membrane after 12 h. However, the optical degree for the Ag-nanogel assembled membranes exhibited considerable reduction for both *S. aureus* and *E. coli*. The results clearly demonstrated that the Ag-nanogel loaded membranes had good effect on the inhibition of the growth for both *S. aureus* (Gram-positive) and *E. coli* (Gram-negative). Meanwhile, the PES/Ag-nanogel exhibited the highest bacterial inhibition ability due to the highest  $\text{Ag}^+$  ions releasing amount in aqueous solution, which was also confirmed by the atomic absorption spectroscopy.

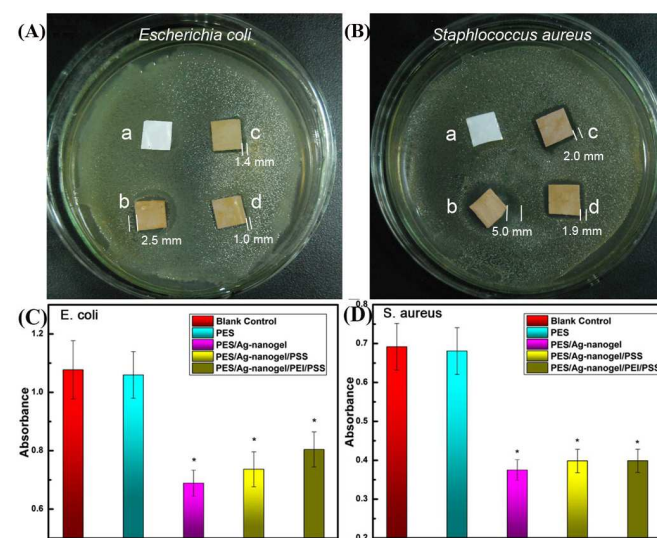


**Figure 9** The inhibition zone picture for (A) *E. coli* (Gram-negative) and (B) *S. aureus* (Gram-positive); a for PES, b for PES/Ag-nanogel, c for PES/Ag-nanogel/PSS, and d for PES/Ag-nanogel/PEI/PSS. The optical degrees for (C) *E. coli* (Gram-negative) and (D) *S. aureus* (Gram-positive), the absorbances represent the bacterial amount after exposure to functionalized membranes for 12 h.

The morphology of adhered bacteria on the Ag-nanogel assembled membranes was further observed by SEM images after bacterial fouling.<sup>62</sup> The pristine PES membrane surface was highly susceptible to bacterial adhesion and colonization. A large amount of bacteria adhered readily on the PES surface, and most of the adhered bacterials aggregated into clusters (Figure 10 (A, a) *E. coli* cells with rod-shape. (E.e) *S. aureus* cells with global shape). For the Ag-nanogel functionalized membranes, the antibacterial adhesion was directly correlated with the coated PSS layers on the substrates. Almost no bacterial cells could be found on the PES/Ag-nanogel surfaces as shown in Fig. 10 (B,F), indicating superior antibacterial functionality of the Ag-nanogel coatings. As for the PES/Ag-nanogel/PSS and PES/Ag-nanogel/PEI/PSS membranes, the antibacterial adhesion ability decreased due to the separation and excellent biocompatibility of PSS coating layer, and also the constructed 3D porous surface may also increase the

affinity of bacterial adhesion. However, compared with the pristine PES membranes, they still exhibited obvious efficiency in antibacterial attachment.

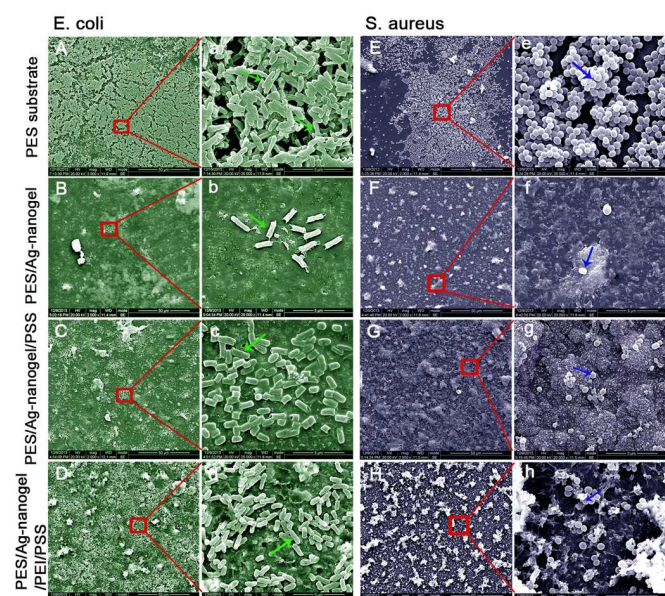


**Figure 10** SEM pictures of *E. coli* (Gram-negative) cultured on the (A) PES, (B) PES/Ag-nanogel, (C) PES/Ag-nanogel/PSS, (D) PES/Ag-nanogel/PEI/PSS. And *S. aureus* (Gram-positive) cultured on the (E) PES, (F) PES/Ag-nanogel, (G) PES/Ag-nanogel/PSS, and (H) PES/Ag-nanogel/PEI/PSS after 24 hours. The membranes (A-H, x2000, the scale bars are 50  $\mu\text{m}$ ; a-h, x20000, the scale bars are 5  $\mu\text{m}$ ).

The results indicated that the obtained Ag-nanogel and heparin-mimicking polymer co-assembled membranes achieved the 3D nanogel assembled morphologies. Compared with recent literatures on surface modification of biomedical membranes, this approach revealed some superior performance in blood compatibility, especially on the declined BFG protein adsorption and greatly suppressed platelet adhesion (barely no platelet adhesion) compared to earlier reports,<sup>48, 63</sup> indicating ultralow thrombotic potential. Another interesting finding is that, with proper biointerface design, the rough membrane surface may own ultralow platelet adhering and activation. Different from many antifouling surface designs,<sup>64, 65</sup> this proposed co-assembly of nanogels and heparin-like polymers combined their anticoagulant and antithrombotic properties. Moreover, besides the antifouling, anticoagulant and antithrombotic properties, the cell cultures experiment demonstrated that the heparin-mimicking membranes can also promote endothelial cells proliferation and influence the cell attachments and morphologies.<sup>32, 47, 52</sup> However, the traditional antifouling membranes via anchor of polymers, such as polyethylene glycol, would inhibit the cell attachments,<sup>65, 66</sup> thus limit the application of modified membranes in tissues engineering.

Furthermore, for the design of antibacterial membrane, such as using antifouling polymers,<sup>67</sup> quaternary ammonium groups contained polymers,<sup>62</sup> and titania composite films,<sup>68</sup> the antibacterial ability, efficiency and durability may be not satisfy long-term *in-vivo* applications of various biomedical membrane

devices. The antibacterial abilities of the antifouling group and quaternary ammonium group immobilized membranes may only effective within the membrane surface and could lost their activity due to the fouling of plasma or bacterial biofilm in long-term usage. The antibacterial effectivity of titanium and its alloys is highly dependent on photostimulation, which may be limited in *in vivo* applications; furthermore, the long-term accumulation toxicity of titanium and its alloys is not completely understood.<sup>69</sup> This paper applied Ag nanoparticle as antibacterial reagent, which may be more efficient for both *E. coli* (gram-negative) and *S. aureus*, (gram-positive) at any environment and exhibit long-term antibacterial ability.<sup>70</sup> Meanwhile, the polymeric nanogels could provide fine surface cover for antibacterial reagents (the direct exposure of Ag NPs presents certain biotoxicity to cells and organs), and also prolong the releasing durability of  $\text{Ag}^+$  ions.

With the mentioned advantages, the co-assembly of Ag-nanogels and heparin-like polymers may pave the way to obtain multifunctional membranes with integrated biocompatibility and antibacterial ability, which could extend the applications of biomedical membranes in various biomedical fields, such as membrane based artificial organs for the treatments of kidney/liver failure, cells and tissues scaffold, and bioreactor for the production of drug and protein.

#### 4. Conclusion

In this study, novel multifunctional biomedical membranes were fabricated by LBL self-assembly of Ag-nanogel and heparin-mimicking polymers. The results indicated that the obtained Ag-nanogel and heparin-mimicking polymer assembled membranes exhibited 3D surface morphologies. The functionalized membrane showed decreased water contact angle, declined protein adsorption, prolonged clotting times, and suppressed platelet adhesion compared to pristine membrane, which indicated the excellent blood compatibility and ultralow thrombotic potential. The cell observation demonstrated that the assembled interface morphology had influence on the cell growth, and the heparin-mimicking membranes showed the best performance in endothelial cells proliferation and cell morphology change. The results of antibacterial study indicated that both the nanogel assembled and heparin-mimicking membranes exhibited significant inhibition capability for *S. aureus* and *E. coli* bacteria. In general, the surface 3D nanogel and heparin-mimicking polymer assembly conferred the modified membranes with integrated blood compatibility, cell proliferation and antibacterial properties for multi-applications; meanwhile, the results also indicated that different surface morphologies and functional groups might present significant influence on the biological properties.

#### Acknowledgements

This work was financially sponsored by the National Natural Science Foundation of China (No. 51173119, and 51225303), and Program for Changjiang Scholars and Innovative Research Team in University (IRT1163). We sincerely acknowledge the financial assistance of visiting research program by the China Scholarship Council (CSC). We should also thank our laboratory members for their generous help, and gratefully

acknowledge the help of Ms. H. Wang, of the Analytical and Testing Center at Sichuan University, for the SEM, and Ms Liang, of the Department of Nephrology at West China Hospital, for the human fresh blood collection.

### Notes and references

<sup>a</sup> College of Polymer Science and Engineering, State Key Laboratory of Polymer Materials Engineering, Sichuan University, Chengdu 610065, China

<sup>b</sup> Department of Chemical Engineering, Department of Biomedical Engineering, University of Michigan, Ann Arbor, Michigan, 48109, USA

<sup>c</sup> National Engineering Research Center for Biomaterials, Sichuan University, Chengdu 610064, China

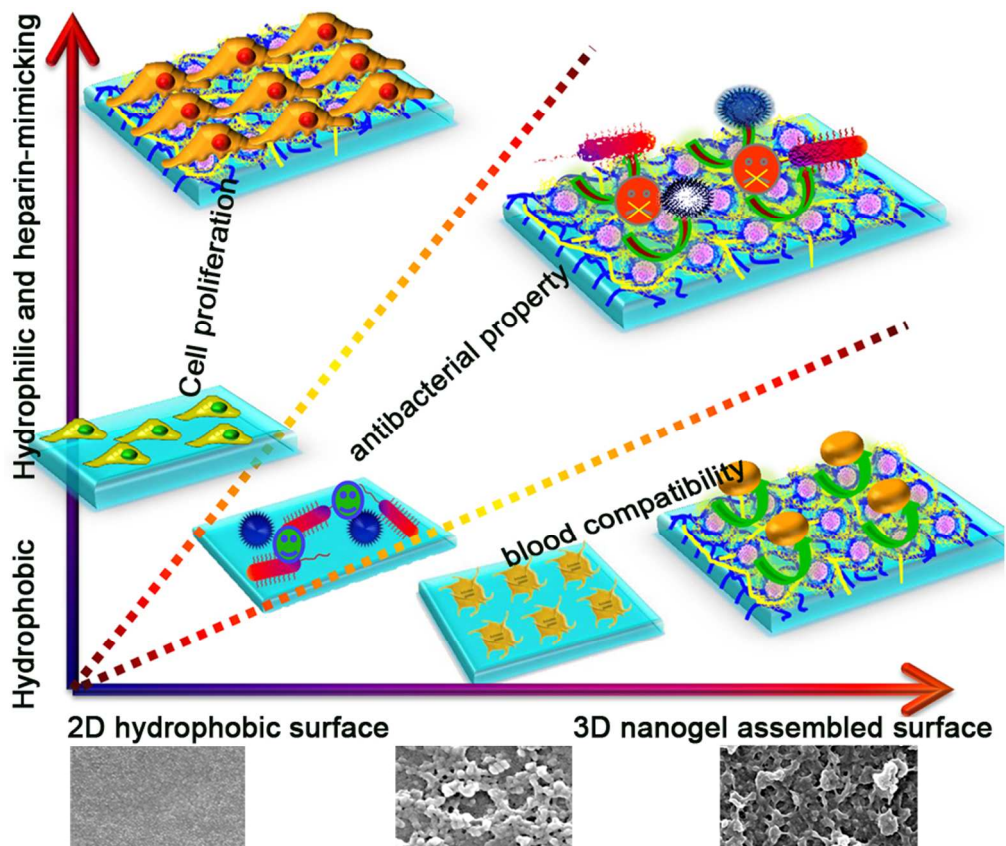
<sup>†</sup> These two authors contribute equally to this work.

\* Corresponding author. Tel: +86-28-85400453, Fax: +86-28-85405402, E-mail: (C. Cheng) sagecheng@163.com or chengcho@umich.edu; (C.S. Zhao) zhaochsh70@163.com or zhaochsh70@scu.edu.cn

† Electronic Supplementary Information (ESI) available: [Detailed information of preparation method, water contact angle, protein adsorption, anticoagulant property of the membranes, platelet adhesion, cell culture, cell morphology on the membranes]. See DOI: 10.1039/b000000x/

- H. Tian, Z. Tang, X. Zhuang, X. Chen and X. Jing, *Prog. Polym. Sci.*, 2012, **37**, 237-280.
- T. T. Ruckh, K. Kumar, M. J. Kipper and K. C. Papat, *Acta Biomater.*, 2010, **6**, 2949-2959.
- C. Zhao, J. Xue, F. Ran and S. Sun, *Prog. Mater. Sci.*, 2013, **58**, 76-150.
- M. P. Lutolf and J. A. Hubbell, *Nat. Biotech.*, 2005, **23**, 47-55.
- J. J. Rice, M. M. Martino, L. De Laporte, F. Tortelli, P. S. Briquez and J. A. Hubbell, *Adv. Healthc. Mater.*, 2013, **2**, 57-71.
- S. Daghighi, J. Sjollem, H. C. van der Mei, H. J. Busscher and E. T. J. Rochford, *Biomaterials*, 2013, **34**, 8013-8017.
- S. H. Lee, M. K. Gupta, J. B. Bang, H. Bae and H.-J. Sung, *Adv. Healthc. Mater.*, 2013, **2**, 908-915.
- D. Rana and T. Matsuura, *Chem. Rev.*, 2010, **110**, 2448-2471.
- D. Depan and R. D. K. Misra, *Acta Biomater.*, 2013, **9**, 6084-6094.
- R. A. Hoshi, R. Van Lith, M. C. Jen, J. B. Allen, K. A. Lapidus and G. Ameer, *Biomaterials*, 2013, **34**, 30-41.
- F. P. Seib, M. Herklotz, K. A. Burke, M. F. Maitz, C. Werner and D. L. Kaplan, *Biomaterials*, 2014, **35**, 83-91.
- Y. Kim, D. Rana, T. Matsuura and W.-J. Chung, *Chem. Commun.*, 2012, **48**, 693-695.
- R. D. K. Misra, C. Nune, T. C. Pesacreta, M. C. Somani and L. P. Karjalainen, *Acta Biomater.*, 2013, **9**, 6245-6258.
- S. Liang, Y. Kang, A. Tiraferri, E. P. Giannelis, X. Huang and M. Elimelech, *ACS Appl. Mater. Interfaces* 2013, **5**, 6694-6703.
- L.-S. Wan, J. Lv, B.-B. Ke and Z.-K. Xu, *ACS Appl. Mater. Interfaces* 2010, **2**, 3759-3765.
- L.-S. Wan, B.-B. Ke, J. Zhang and Z.-K. Xu, *J. Phys. Chem. B*, 2011, **116**, 40-47.
- P. Zhang, H. Wu, H. Wu, Z. Lù, C. Deng, Z. Hong, X. Jing and X. Chen, *Biomacromolecules*, 2011, **12**, 2667-2680.
- M. Rouabhia, H. Park, S. Meng, H. Derbali and Z. Zhang, *PLoS One* 2013, **8**, e71660.
- D. Depan, T. C. Pesacreta and R. D. K. Misra, *Biomater. Sci.*, 2014, **2**, 264-274.
- C. Cheng, L. Ma, D. F. Wu, J. Ren, W. F. Zhao, J. M. Xue, S. D. Sun and C. S. Zhao, *J. Membr. Sci.*, 2011, **378**, 369-381.
- M. L. Steen, A. C. Jordan and E. R. Fisher, *J. Membr. Sci.*, 2002, **204**, 341-357.
- H. Faber, J. Hirschmann, M. Klauünzer, B. r. Braunschweig, W. Peukert and M. Halik, *ACS Appl. Mater. Interfaces* 2012, **4**, 1693-1696.
- S. Theapsak, A. Watthanaphanit and R. Rujiravanit, *ACS Appl. Mater. Interfaces* 2012, **4**, 2474-2482.
- D. Tan, X. Zhang, J. Li, H. Tan and Q. Fu, *J. Biomed. Mater. Res. A*, 2012, **100**, 380-387.
- X. J. Huang, D. Guduru, Z. K. Xu, J. Vienken and T. Groth, *Macromol. Biosci.*, 2011, **11**, 131-140.
- Y. Chang, W.-J. Chang, Y.-J. Shih, T.-C. Wei and G.-H. Hsiue, *ACS Appl. Mater. Interfaces* 2011, **3**, 1228-1237.
- J.-H. Jiang, L.-P. Zhu, X.-L. Li, Y.-Y. Xu and B.-K. Zhu, *J. Membr. Sci.*, 2010, **364**, 194-202.
- P.-C. Chen, L.-S. Wan and Z.-K. Xu, *J. Mater. Chem.*, 2012, **22**, 22727-22733.
- Y.-H. Zhao, B.-K. Zhu, L. Kong and Y.-Y. Xu, *Langmuir*, 2007, **23**, 5779-5786.
- Y.-F. Zhao, L.-P. Zhu, Z. Yi, B.-K. Zhu and Y.-Y. Xu, *J. Membr. Sci.*, 2013, **440**, 40-47.
- C. Zhao, J. Xue, F. Ran and S. Sun, *Prog. Mater. Sci.*, 2012, **58**, 76-150.
- Y. Xia, X. He, M. Cao, C. Chen, H. Xu, F. Pan and J. R. Lu, *Biomacromolecules*, 2013, **14**, 3615-3625.
- Z. Tang, Y. Wang, P. Podsiadlo and N. A. Kotov, *Adv. Mater.*, 2006, **18**, 3203-3224.
- N. Joseph, P. Ahmadiannamini, R. Hoogenboom and I. F. J. Vankelecom, *Polym. Chem.*, 2014, DOI: 10.1039/c3py01262j.
- D. G. Yu, W. C. Lin and M. C. Yang, *Bioconjugate Chem.*, 2007, **18**, 1521-1529.
- H. X. Yu, Y. T. Zhang, X. B. Sun, J. D. Liu and H. Q. Zhang, *Chem. Eng. J.*, 2014, **237**, 322-328.
- M. J. Serpe, K. A. Yarmey, C. M. Nolan and L. A. Lyon, *Biomacromolecules*, 2004, **6**, 408-413.
- K. Ogawa, B. Wang and E. Kokufuta, *Langmuir*, 2001, **17**, 4704-4707.
- J. J. Panda and V. S. Chauhan, *Polym. Chem.*, 2014, **5**, 4418-4436.
- S. Rejinold N, K. P. Chennazhi, H. Tamura, S. V. Nair and J. Rangasamy, *ACS Appl. Mater. Interfaces* 2011, **3**, 3654-3665.
- W. Wu, T. Zhou, A. Berliner, P. Banerjee and S. Zhou, *Chem. Mater.*, 2010, **22**, 1966-1976.
- J. Liu, C. Detrembleur, M. Hurtgen, A. Debuigne, M.-C. De Pauw-Gillet, S. Mornet, E. Duguet and C. Jerome, *Polym. Chem.*, 2014, DOI: 10.1039/C4PY00352G.
- S. Cuenot, S. Radji, H. Alem, S. Demoustier-Champagne and A. M. Jonas, *Small*, 2012, **8**, 2978-2985.
- V. Thomas, M. M. Yallapu, B. Sreedhar and S. K. Bajpai, *J. Colloid Interface Sci.*, 2007, **315**, 389-395.
- P. S. K. Murthy, Y. Murali Mohan, K. Varaprasad, B. Sreedhar and K. Mohana Raju, *J. Colloid Interface Sci.*, 2008, **318**, 217-224.
- Z.-m. Xiu, Q.-b. Zhang, H. L. Puppala, V. L. Colvin and P. J. J. Alvarez, *Nano Lett.*, 2012, **12**, 4271-4275.
- S. Nie, M. Tang, C. Cheng, Z. Yin, L. Wang, S. Sun and C. Zhao, *Biomater. Sci.*, 2014, **2**, 98-109.

48. L. Ma, H. Qin, C. Cheng, Y. Xia, C. He, C. Nie, L. Wang and C. Zhao, *J. Mater. Chem. B*, 2014, **2**, 363-375.
49. J. Pan, Y. Qian, X. Zhou, A. Pazandak, S. B. Frazier, P. Weiser, H. Lu and L. Zhang, *Nat. Biotechnol.*, 2010, **28**, 203-207.
50. L. L. Li, C. Cheng, T. Xiang, M. Tang, W. F. Zhao, S. D. Sun and C. S. Zhao, *J. Membr. Sci.*, 2012, **405**, 261-274.
51. C. Cheng, S. Li, S. Nie, W. Zhao, H. Yang, S. Sun and C. Zhao, *Biomacromolecules*, 2012, **13**, 4236-4246.
52. R. Mammadov, B. Mammadov, S. Toksoz, B. Aydin, R. Yagci, A. B. Tekinay and M. O. Guler, *Biomacromolecules*, 2011, **12**, 3508-3519.
53. C. Cheng, S. Nie, S. Li, H. Peng, H. Yang, L. Ma, S. Sun and C. Zhao, *J. Mater. Chem. B*, 2013, **1**, 265-275.
54. C. Cheng, S. Li, W. Zhao, Q. Wei, S. Nie, S. Sun and C. Zhao, *J. Membr. Sci.*, 2012, **417-418**, 228-236.
55. J. L. Brash and T. A. Horbett, *ACS Symp. Ser.*, ACS Publications:1995, 1-25.
56. K. Ishihara, K. Fukumoto, Y. Iwasaki and N. Nakabayashi, *Biomaterials*, 1999, **20**, 1553-1559.
57. M. M. Flanders, R. Crist and G. M. Rodgers, *Clin. Chem.*, 2003, **49**, 169-172.
58. M. B. Gorbet and M. V. Sefton, *Biomaterials*, 2004, **25**, 5681-5703.
59. R. Rajaraman, D. Rounds, S. Yen and A. Rembaum, *Exp. Cell Res.*, 1974, **88**, 327-339.
60. Y. Sakai and K. Nakazawa, *Acta Biomater.*, 2007, **3**, 1033-1040.
61. X. L. Cao, C. Cheng, Y. L. Ma and C. S. Zhao, *J. Mater. Sci. Mater. Med.*, 2010, **21**, 2861-2868.
62. W. J. Yang, D. Pranantyo, K.-G. Neoh, E.-T. Kang, S. L.-M. Teo and D. Rittschof, *Biomacromolecules*, 2012, **13**, 2769-2780.
63. H. Zhou, C. Cheng, H. Qin, L. Ma, C. He, S. Nie, X. Zhang, Q. Fu and C. Zhao, *Polym. Chem.*, 2014, **5**, 3563-3575.
64. Q. Wei, T. Becherer, P.-L. M. Noeske, I. Grunwald and R. Haag, *Adv. Mater.*, 2014, **26**, 2688-2693.
65. A. T. Neffe, M. von Ruesten-Lange, S. Braune, K. Lutzow, T. Roch, K. Richau, A. Kruger, T. Becherer, A. F. Thunemann, F. Jung, R. Haag and A. Lendlein, *J. Mater. Chem. B*, 2014, **2**, 3626-3635.
66. C.-J. Pan, Y.-H. Hou, B.-B. Zhang, Y.-X. Dong and H.-Y. Ding, *J. Mater. Chem. B*, 2014, **2**, 892-902.
67. S. Yuan, D. Wan, B. Liang, S. O. Pehkonen, Y. P. Ting, K. G. Neoh and E. T. Kang, *Langmuir*, 2011, **27**, 2761-2774.
68. R. Venkatasubramanian, R. S. Srivastava and R. D. K. Misra, *Mater. Sci. Technol.*, 2008, **24**, 589-595.
69. D. Zheng, K. G. Neoh, Z. Shi and E.-T. Kang, *J. Colloid Interface Sci.*, 2013, **406**, 238-246.
70. E. Fortunati, S. Mattioli, L. Visai, M. Imbriani, J. L. G. Fierro, J. M. Kenny and I. Armentano, *Biomacromolecules*, 2013, **14**, 626-636.



This study presents fabrication of multifunctional nanolayer on biomedical membrane surface by using LBL self-assembly of nanogels and heparin-like polymers, which confers the modified membranes own integrated blood compatibility, cell proliferation and antibacterial properties  
 88x74mm (300 x 300 DPI)